About mechanically induced crystallization kinetics in filled natural rubber

Anthony Le Bihan, Yann Marco, V. Le Saux, Laurent Chazeau, Jean-Marc Chenal, Iona Warneboldt, Clément Champy, Pierre Charrier

About mechanically induced crystallization kinetics in filled natural rubber

A. Le Bihan, Y. Marco, V. Le Saux
ENSTA Bretagne, UMR CNRS 6027, IRDL, 29806 Brest, France

L. Chazeau, J.-M. Chenal
INSA Lyon, UMR CNRS 5510, MATEIS, 69621 Villeurbanne, France

I. Warneboldt, P. Charrier, C. Champy
Vibracoustic Nantes, CAE and Durability Prediction Department, 44474 Carquefou, France

ABSTRACT: In this work, we provide information about mechanically induced crystallization (MIC) kinetics. First, we show that the usual definition of threshold elongations for crystallization and melting does not always make sense. We then show the effect of the loading path on the crystallization levels reached. Finally, we define a quantity representative of the crystallization kinetics and try to describe it using quantities as elongation or stress. At the same time, we illustrate that crystallization is a self-regulating phenomenon: a saturation of crystallization kinetics can be reached.

1 INTRODUCTION

Natural Rubber (NR) is widely used in automotive anti-vibration parts due to its exceptional damping and vibration resistance properties: it's an ideal material for reducing unwanted vibrations from the road, engines, suspension or other components. NR is also known for its excellent fatigue properties.

Automotive parts are subjected to very complex loading conditions. For NR, so-called non-relaxing conditions lead to local reinforcement of the material, resulting in increased fatigue (Cadwell et al., 1940). This increase in service life can be graphically illustrated by a HAIGH diagram: iso-curves of lifetime in a mean-amplitude load plane. Such diagram is charaterized by a bell curve (Champy et al., 2021).

This local reinforcement effect is characteristic of NR and its ability to crystallize under tension due to its stereoregularity (Huneau, 2011). In reality, the increase in lifetime duration is merely a consequence of other phenomena that occur during cracking. One of the first investigations into the effect of non-relaxing loading on crack propagation was that of (Busse, 1935). He observed that the main crack, initially orthogonal to the loading direction, gives rise to two new cracks. These tend to orient themselves parallel to the loading direction or turn back for highly non-relaxing loading. A second effect related to crack propagation was observed by (Saintier, Cailletaud, and Piques, 2011; Warneboldt et al., 2022): crack branching *i.e.* ramification near the main crack. The crack propagates in a direction perpendicular to the loading direction.

Crystallization kinetics is also fundamental to explain the hysteretic behaviour observed under dynamic conditions which leads to the reinforcement and the lifetime increase. Usually, to better understand crystallization kinetics, the main idea is to stretch the material to a given strain and follow the evolution of the crystallinity index, usually by Wide Angle X-Ray Diffraction (WAXD) measurements. (Brüning et al., 2015) studied the evolution of crystallization during relaxation, at different temperatures and for different imposed strains. This crystallization follow-up was carried out over short times, of the order of a minute. More recently, (Albouy and Sotta, 2020) performed the same exercise over longer times (one hour) at ambient temperature. In particular, they have shown that, over a given imposed elongation, there is an independence of crystallization kinetics to the imposed elongation. They also proved the existence of a time-strain equivalence that may be used to model crystallization (Sotta and Albouy, 2020).

These first data provide a better understanding of the kinetic effects and also raise some questions: how does crystallization kinetics evolve? It is possible to easily relate it to simple quantities such as elongation or stress? Kinetics established by (Albouy and

Sotta, 2020) are given for a monotonic loading, but how would kinetics vary if the loading path is different? In order to answer some of these questions, we chose to realize an anhysteretic (ANH) test and simple tension tests under synchrotron beam. The results of the two kinds of tests are analyzed and compared.

The paper is organized as follows. Section 2 describes the studied material and the experimental set-up. Section 3 presents the experiments and the data analysis procedure. Section 4 is devoted to the results discussion. Section 5 concludes and gives perspectives for this work.

2 MATERIALS AND EXPERIMENTAL SET-UP

2.1 *Materials and specimen*

The material of interest is an industrial filled at 42 phr of carbon black and vulcanized natural rubber. The basic formulation is given in Table 1.

Component	Content [phr]
Matrix	100
Fillers	42
Zinc Oxyde	4
Plasticizer	5
Stearic acid	2
Antioxidant	2
Antiozonant	2
Accelerator	0,6
Sulfur	2,8

Table 1: Recipe of the material

The specimens were all manufactured under identical molding process settings and from a single material batch to ensure equal mixing and curing conditions. Samples used are called mini PureShear, see Figure 1. The 1mm thickness is a good compromise for WAXD experiments, between X-ray absorption and X-ray scattering. The specimen lengths used vary between 5 and 10 mm to ensure uniaxial tension conditions.

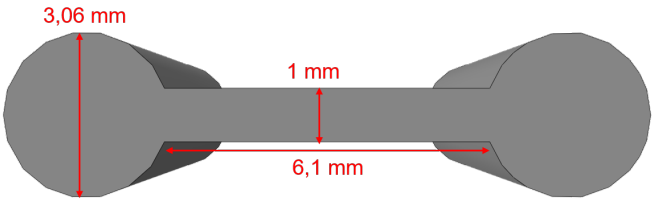

Figure 1: mini-PureShear sample dimensions

2.2 *Synchrotron beamline*

The in-situ WAXD experiments were performed on the D2AM beamline at the European Synchrotron Radiation Facility. The X-Ray energy is 8 keV corresponding to a wavelength of 1,54 Å and the beam size is 300 μm$\times$ 200 μm.

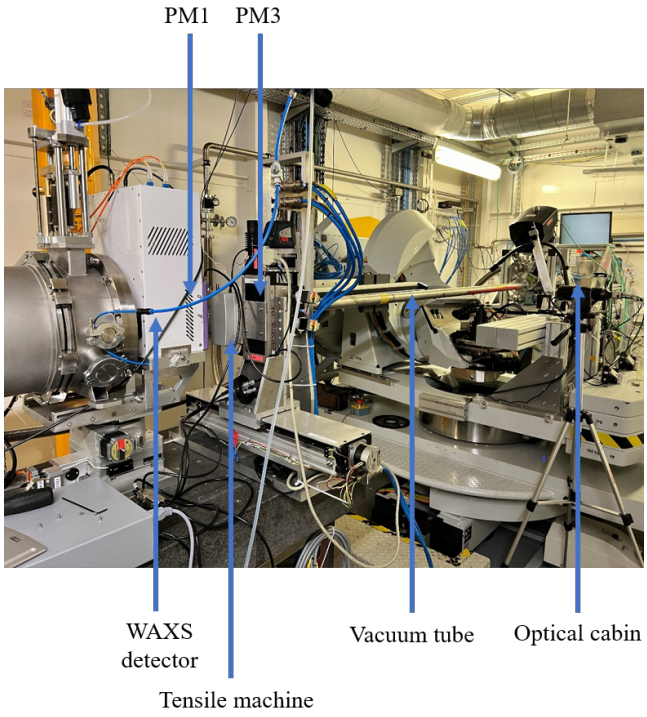

Figure 2: Line disposition: beam, machine and WAXD detector

Two important Positive Intrinsic Negative (PIN) diodes, called PM, are visible on the Figure 2. The PM3 is located at the exit of the optical cabin and is used to measure the intensity of the incident beam. The PM1 is located at the center of the WAXD detector, and is used to measure the intensity of the transmitted beam.

The WAXD sensor used is a strip sensor and its surface area is 1340×700 pixels. Each pixel size is 13μm and measures a quantity proportional to the number of photons received by that pixel.

The used tensile machine is LINKAM MODULE FORCE STAGE allowing displacement driving. The specificity of this machine is a space along the axis perpendicular to the sample: the machine lets an X-ray beam pass through itself as well as through the sample.

3 TEST PROCEDURE

3.1 *Mechanical signals*

All the tests are driven by crosshead displacement. Several types of tests are considered. First, classic load-unload tests were carried out between $\lambda = 1$ and $\lambda = 5.5$ where λ is the stretch of the material in the tensile direction. The three elongation rates investigated are: $\dot{\lambda}_1 = 5 \times 10^{-1}$ s^{-1}, $\dot{\lambda}_2 = 5 \times 10^{-2}$ s^{-1}, $\dot{\lambda}_3 = 5 \times 10^{-3}$ s^{-1}.

Another test performed is the anhysteretic (ANH) or multi-relaxation test. The principle is to apply to the sample a low stretch, then relax it at this constant stretch, then repeat the process for increasing elongations until the maximum elongation. Stretching rate and relaxation time are kept the same during the full

test. Once maximum elongation has been reached, the same process is repeated during the unload. The elongation increment is $\Delta\lambda = 0.3$, the phase duration of each relaxation is $\Delta t = 60$ seconds, the incremental strain rate is $\dot{\lambda}_2 = 5 \times 10^{-2}\ \mathrm{s}^{-1}$, the minimal elongation $\lambda_{\min} = 1.0$ and the maximal one is $\lambda_{\max} = 5.5$. A representative scheme of these two tests is proposed in Figure 3.

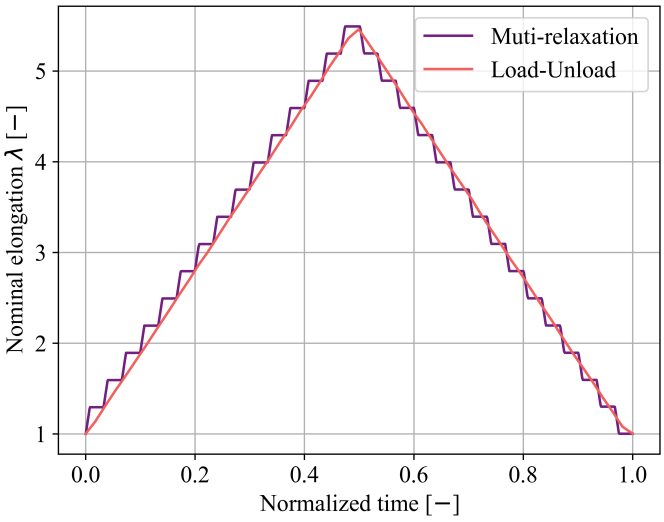

Figure 3: Test procedures for performed tests (normalized time)

3.2 *Background correction and post-treatment*

A raw diffraction pattern issued from the WAXD sensor cannot be analyzed as it stands. Although a diffraction pattern $I_{d,raw}$ and a PM1 value, $I_{1,raw}$, can be obtained from a measurement, several factors hamper its analysis. First, the air between the exit of the optical cabin and the WAXD detector is diffracted by the electrons. Then, during a mechanical test, the specimen is stretched and its thickness varies.

To subtract the air diffraction, it is common to measure the *background* diffraction: a measurement without any specimen, where only the air is diffracted. A diffraction pattern, $I_{d,bck}$, and a PM1 value, $I_{1,bck}$, are therefore recorded. Then, in order to overcome all the biases mentioned above, it is necessary to apply successive BEER-LAMBERT laws and, assuming the incompressibility of the material when uniaxially stretched, it is then possible to obtain the following correction formula (Ran et al., 2001; Beurrot-Borgarino et al., 2013):

$$\frac{1}{\sqrt{\lambda}}\left(\frac{I_{d,raw}}{I_{1,raw}} - \frac{I_{d,bck}}{I_{1,bck}}\right) \tag{1}$$

Applying this correction formula to a raw diffraction pattern obtained from the WAXD detector typically produces the pattern shown in Figure 4.

It shows the three ZnO rings at large angles, the amorphous halo and the classic crystalline peaks found in industrially formulated natural rubbers. (120) and (200) peaks in the direction orthogonal to the tensile direction and the (201) peak between these two directions (Beurrot-Borgarino et al., 2013; Candau et al., 2012; Huneau, 2011; Albouy and Sotta, 2020). A post-processing based on deconvolution is then carried out to distinguish the diffraction of the crystalline phase from the amorphous one: the areas diffracted by these phases are called $\mathscr{I}_{\mathrm{crist}}$ and $\mathscr{I}_{\mathrm{amo}}$ respectively.

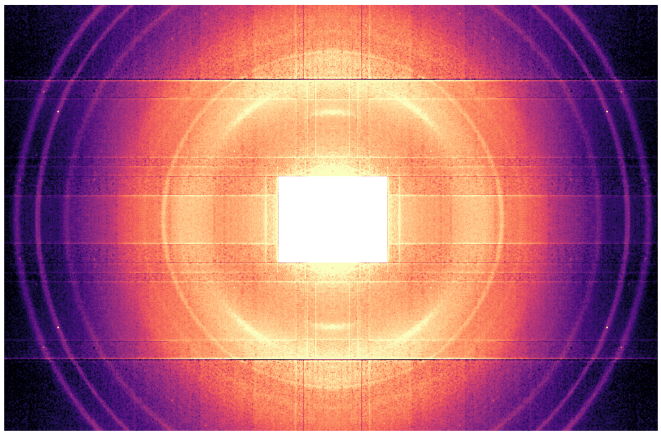

Figure 4: Typical diffraction pattern (tension direction is horizontal)

The next step is to estimate a crystallinity index: the volumetric fraction of the crystallized phase within the material. Several definitions exist in the literature. The definition used here is (Beurrot-Borgarino et al., 2013):

$$\chi_c = \frac{\mathscr{I}_{crist}}{\mathscr{I}_{crist} + \mathscr{I}_{amo}} \tag{2}$$

4 RESULTS

The results are all extracted from the same ESRF campaign (Le Bihan et al., 2023).

4.1 *Load-unload tests*

The three load-unload curves in the elongation *vs.* cristallinity index plane (λ, χ_c), are plotted in Figure 5. It is possible to extract the elongations at the onset of crystallization, λ_C and melting λ_M. These are presented in the Table 2.

Strain rate [s^{-1}]	$\dot{\lambda}_3$	$\dot{\lambda}_2$	$\dot{\lambda}_1$
λ_C	2,7	3,0	3,1
λ_M	2,3	2,2	2,2

Table 2: Evolution of threshold elongations with strain rate

The melting threshold elongation λ_M of crystallites varies little or not at all with the strain rate, matching with (Albouy and Sotta, 2020) and seems to converge towards 2.2 . On the other hand, the elongation at the onset of crystallization increases with $\dot{\lambda}$, in line with (Albouy and Sotta, 2020; Candau et al., 2015).

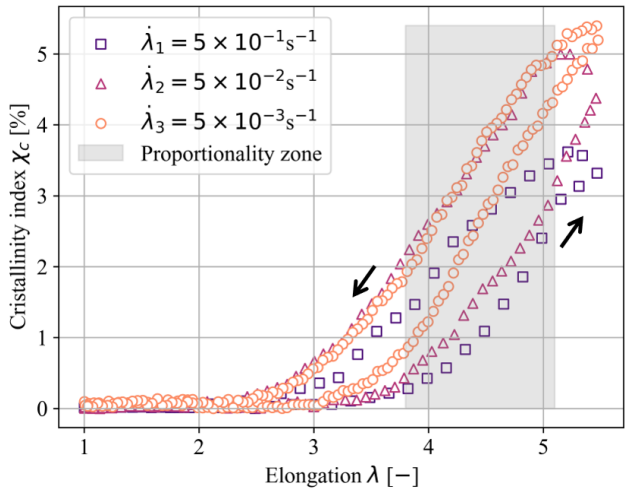

Figure 5: Load-unload curves for the three different strain rates

The Figure 5 shows that crystallization is "delayed": a maximum elongation does not correspond to a maximum of crystallinity. In fact, the crystallinity index continues to increase during the beginning of the unload phase, then decreases. The higher the strain rate, the more pronounced the overshoot. For a given stretch, a slower strain rate leads to a higher crystallinity index.

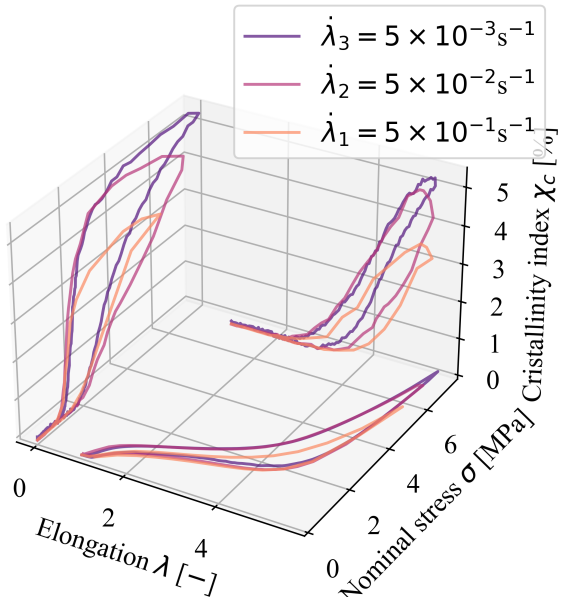

Figure 6: Point cloud $(\lambda, \sigma, \chi_c)$ projections for the 3 strain rates

Figure 6 highlights three coupling hysteresis loops: stress to strain, crystallization to strain and crystallization to stress.

It is possible to describe cristallinity *versus* time or cristallinity *versus* stress curves by linear approximation. On some well chosen elongation ranges (grey zone of the Figure 5), this linear approximation is justified: when MIC appears, it seems to be proportional to elongation. The performed approximations are:

$$\chi_c = \frac{\partial \chi_c}{\partial t} \times t + \chi_c(t_0) \tag{3}$$

$$\chi_c = \frac{\partial \chi_c}{\partial \sigma} \times \sigma + \chi_c(\sigma_0) \tag{4}$$

where slopes $\frac{\partial \chi_c}{\partial t}$ and $\frac{\partial \chi_c}{\partial \sigma}$ are representative of crystallization kinetics (regarding time or nominal stress) and $\chi_c(t_0)$ and $\chi_c(\sigma_0)$ describe the cristallinity index at the beginning of the step. Conventional cycles at the three strain rates permits to define crystallization kinetics for load and melting kinetics for unload. These kinetics are presented in Table 3.

	$\frac{\partial \chi_c}{\partial t}$ [%/s]		$\frac{\partial \chi_c}{\partial \sigma}$ [%/MPa]	
Strain rate	Load	Unload	Load	Unload
$\dot{\lambda}_1$	1,440	−1,159	0,898	3,099
$\dot{\lambda}_2$	0,155	−0,149	0,830	3,174
$\dot{\lambda}_3$	0,018	−0,016	0,987	3,180

Table 3: Kinetics of crystallization (or melting) for simple cycles

4.2 *Comparison of anhysteretic test and conventional cycles*

Figure 7 shows evolution of nominal stress and crystallinity index *versus* elongation for ANH tests. Be careful which way these curves are read. For stress, the load curve is "above" the unload curve. For crystallization, it's the opposite. At each stress relaxation

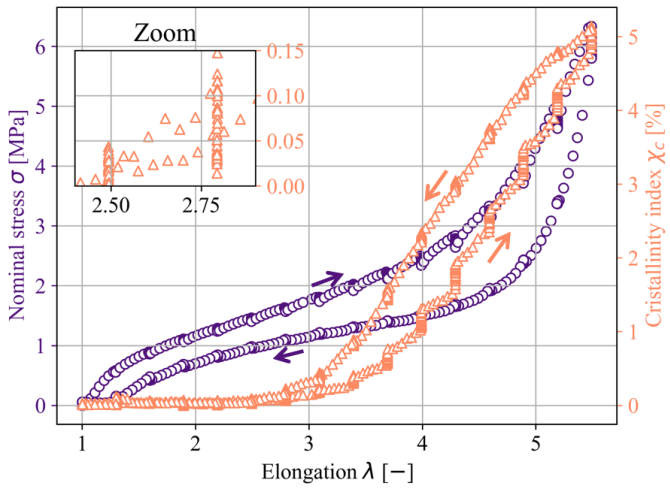

Figure 7: stress and cristallinity index curves for ANH test

step, whether load or unload, crystallinity increases. At first sight, one might wonder what effect the stress relaxation steps have on crystallization *i.e.* the effect of the test duration. A suitable comparison test would be a load-unload at the same draw ratio rate, $\dot{\lambda}_2$. We use the test performed in section 4.1, at $\dot{\lambda}_2$ and $\dot{\lambda}_3$ and compare both types of tests on Figure 8.

At each relaxation stage of the load, the ANH curve starts from the simple curve at $\dot{\lambda}_2$ and ends at the simple curve at $\dot{\lambda}_3$. On the other hand, the overall melting kinetic does not seem to be affected by time effect. Still on the global considerations, it was previously established that the onset elongation for the start of crystallization, λ_C, was 3.0 for a strain rate $\dot{\lambda}_2 = 5{,}0 \times 10^{-2}\ \text{s}^{-1}$ (see Table 2). For the ANH test,

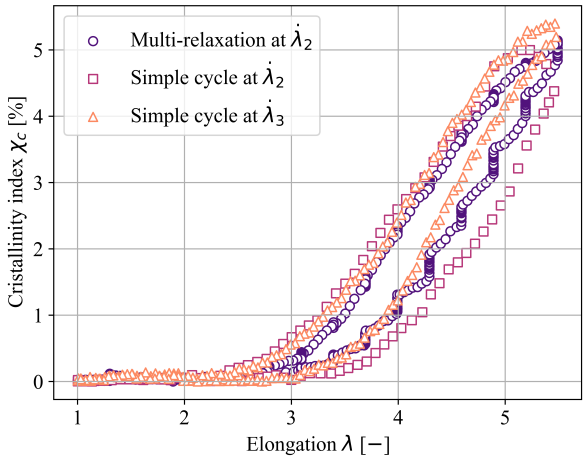

Figure 8: Comparison of ANH test with simple cycles

the onset of crystallization is detected at $\lambda = 2.6 < \lambda_C$. The relaxation time allows the material to crystallize before reaching the threshold elongation λ_C. The same phenomenon occurs at the end of the test, when crystallisation is detected for $\lambda < \lambda_M$. This directly questions the relevance of the definition of threshold elongations. For dynamic test, it is well known that MIC only appears when $\lambda > \lambda_C$ and disappears when $\lambda < \lambda_M$. However, thanks to time effects, this ANH test shows that it is possible to induce mechanical crystallization outside the interval $[\lambda_M; \lambda_C]$.

This test also provides an answer about the effect of thermomechanical history on crystallization kinetics: for a given elongation, which loading path leads to the highest crystallinity indices: continuous loading (conventional cycle) or with intermediate relaxation steps (ANH test)? It appears that giving the material more time does not lead to a significant increase of the crystallinity index. The main difference is the absence of overshoot in the ANH test, since the relaxation steps have modified the crystallization kinetics during the loading phase, especially at the highest stretching levels before.

4.3 *MIC kinetics during ANH test*

Figures 9 to 12 represents cristallinity index χ_c and crystallization kinetics evaluated by equation (3) or (4) during loading phase (from $\lambda_{\min}$ to $\lambda_{\max}$) or unloading phase (from $\lambda_{\max}$ to $\lambda_{\min}$).

On the temporal curves of Figures 9 and 10, it can be seen that the crystallization kinetics increase with elongation until a saturation is reached, as classically observed on AVRAMI curves (Avrami, 2004): MIC kinetics is a self-regulating phenomenon. If we look at the values of these kinetics, there is a clear difference between the loading (or unloading) phases and the relaxation phases: we can clearly see a difference of a factor of 10 regarding kinetics between the two types of steps. We can also compare the kinetics obtained during the ANH test with those obtained for simple cycles (see Table 3). In terms of crystallisation kinetics, relaxation steps appear to be negligible, but in terms of crystallinity index, they still lead to a significant increase. On the other hand, the crystallization kinetics values of the loadings steps of the ANH test correspond to those obtained for a simple cycle performed under a ten times lower tension speed ($\partial\chi_c/\partial t = 0.018$%/s for $\dot{\lambda}_3$ in Table 3): it show that, although at first sight relaxation steps have almost no effect on the final crystallinity indexes reached but they have a significant impact on the crystallisation kinetics.

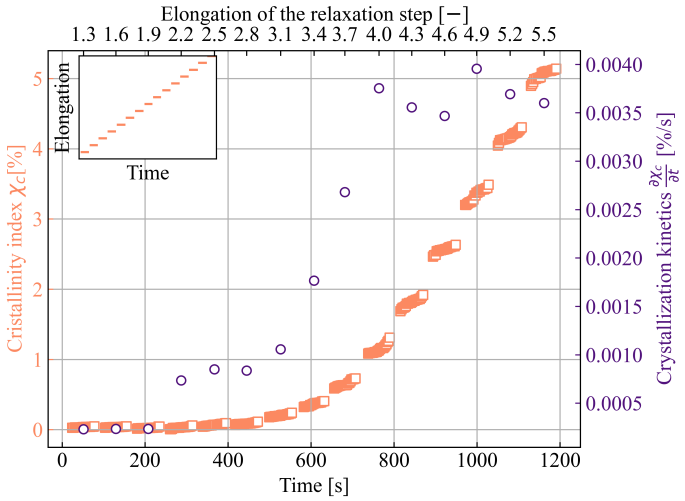

Figure 9: Cristallinity index (□) and kinetics (◯) *vs.* time during relaxation steps of the loading phase (ANH test)

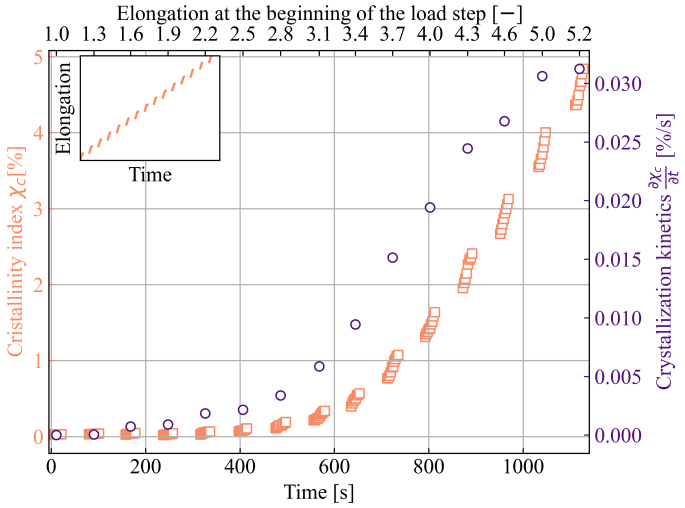

Figure 10: Cristallinity index (□) and kinetics (◯) *vs.* time during loading steps of the loading phase (ANH test)

Figures 9 and 10 indirectly show that elongation is not an unifying variable for crystallization kinetics. Would nominal stress be? Figures 11 and 12 show that the nominal stress cannot unify the kinetics, otherwise the slope $\partial\chi_c/\partial\sigma$ would be constant. What is worth noting, however, is that it exists a nominal stress that leads to an optimum of crystallization or melting kinetics, in both the loading (Figure 11) and unloading (Figure 12) phases.

Regarding melting kinetics values, while those obtained on the simple cycles seemed to stagnate at

around 3.1 %/MPa (see Table 3), those obtained on the ANH test are clearly dependent on the nominal stress, although of the same order of magnitude (see Figure 12).

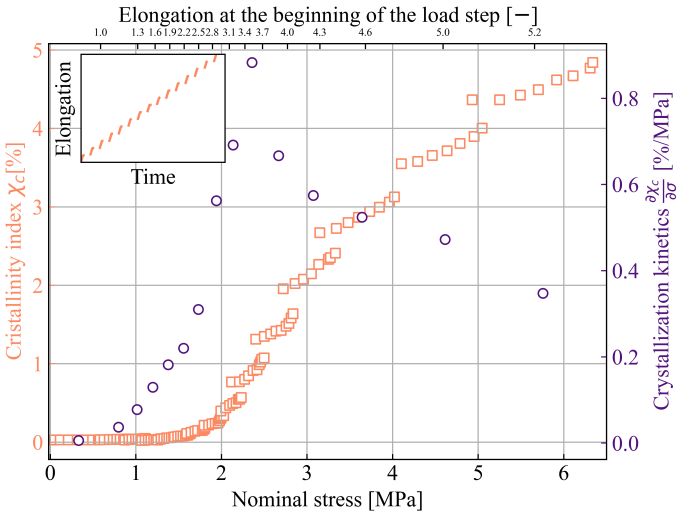

Figure 11: Cristallinity index (□) and kinetics (◯) *vs.* nominal stress during loading steps of the loading phase (ANH test)

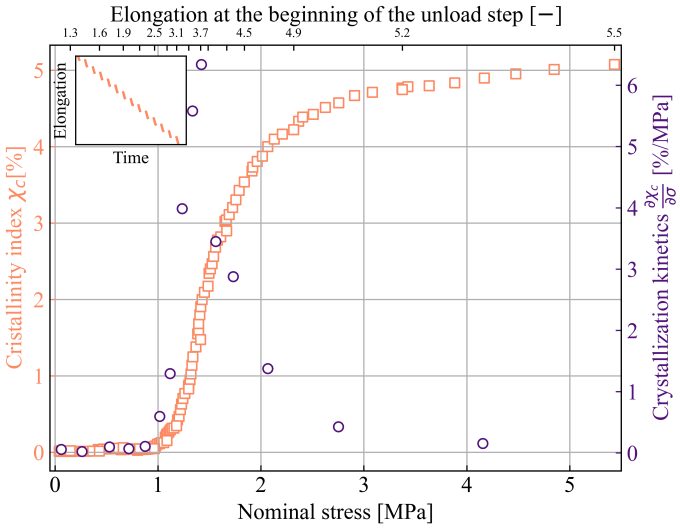

Figure 12: Cristallinity index (□) and kinetics (◯) *vs.* nominal stress during unloading steps of the unloading phase (ANH test)

5 CONCLUSIONS AND PERSPECTIVES

The ANH test confirms that the classic definitions of threshold elongations for crystallization and melting should be treated with caution: it is possible to obtain crystallization at very small stretches by giving time to the material to crystallize.

The ANH test also shows that the crystallization kinetics are higher during the loading or unloading phases than during the relaxation phases. For the strain rates tested, the test also demonstrates a saturation of the crystallization kinetics. The various graphical representations show that the unification of kinetics (by time, strain or stress) is not straight forward. The comparison of a simple cycle (monotonic loading) with an ANH test (interrupted loading) shows that the loading path has almost no effect on the final crystallinity indexes.

This ANH test has provided a lot of answers about the notions of crystallization kinetics, but it also raises many questions: for the ANH test, what would happen if the draw ratio were different? if there were fewer relaxation steps? if there were longer relaxation steps? or creep steps instead of relaxation ones?

REFERENCES

Albouy, P.-A. and Sotta, P. “Draw Ratio at the Onset of Strain-Induced Crystallization in Cross-Linked Natural Rubber”. *Macromolecules* 53, no. 3 (2020): 992–1000.

Avrami, M. “Kinetics of Phase Change. II Transformation-Time Relations for Random Distribution of Nuclei”. *The Journal of Chemical Physics* 8, no. 2 (2004): 212–224. Visited on 01/23/2024.

Beurrot-Borgarino, S. et al. “Strain-Induced Crystallization of Carbon Black-Filled Natural Rubber during Fatigue Measured by in Situ Synchrotron X-ray Diffraction”. *International Journal of Fatigue* 47 (2013): 1–7.

Brüning, K. et al. “Kinetics of Strain-Induced Crystallization in Natural Rubber: A Diffusion-Controlled Rate Law”. *Polymer* 72 (2015): 52–58.

Busse, W. F. “Tear Resistance and Structure of Rubber”. *Rubber Chemistry and Technology* 8, no. 1 (1935): 122–137.

Cadwell, S. M. et al. “Dynamic Fatigue Life of Rubber”. *Industrial & Engineering Chemistry Analytical Edition* 12, no. 1 (1940): 19–23.

Candau, N. et al. “Characteristic-Time of Strain Induced Crystallization of Crosslinked Natural Rubber”. *Polymer* 53, no. 13 (2012): 1423–1464.

Candau, N. et al. “Influence of Strain Rate and Temperature on the Onset of Strain Induced Crystallization in Natural Rubber”. *European Polymer Journal* 64 (2015): 244–252.

Champy, C. et al. “Fatigue of Crystallizable Rubber: Generation of a Haigh Diagram over a Wide Range of Positive Load Ratios”. *International Journal of Fatigue* 150 (2021): 106313.

Huneau, B. “Strain-Induced Crystallization of Natural Rubber: A Review of X-ray Diffraction Investigations”. *Rubber Chemistry and Technology* 84, no. 3 (2011): 425–452.

Le Bihan, A. et al. (Influence of the Loading History on Strain Induced Cristallisation of Elastomers with Original Architecture of Crosslinks Network - https://doi.esrf.fr/10.15151/ESRF-ES-1191261152. In collab. with Gilbert Chahine and Isabelle Morfin). 2023.

Ran, S. et al. “Structural Changes during Deformation of Kevlar Fibers via On-Line Synchrotron SAXS/WAXD Techniques”. *Polymer* 42, no. 4 (2001): 1601–1612.

Saintier, N., Cailletaud, G., and Piques, R. “Cyclic Loadings and Crystallization of Natural Rubber: An Explanation of Fatigue Crack Propagation Reinforcement under a Positive Loading Ratio”. *Materials Science and Engineering: A* 528, no. 3 (2011): 1078–1086.

Sotta, P. and Albouy, P.-A. “Strain-Induced Crystallization in Natural Rubber: Flory’s Theory Revisited”. *Macromolecules* 53, no. 8 (2020): 3097–3109.

Warneboldt, I. et al. “Experimental Investigations about Complex Non-Relaxing Fatigue Loads for Carbon-Black Filled Natural Rubber”. *International Journal of Fatigue* 156 (2022): 106696.